

This is the accepted manuscript made available via CHORUS. The article has been published as:

## Diffusion and interface growth in hafnium oxide and silicate ultrathin films on Si(001)

L.V. Goncharova, M. Dalponte, T. Feng, T. Gustafsson, E. Garfunkel, P.S. Lysaght, and G. Bersuker

Phys. Rev. B **83**, 115329 — Published 25 March 2011

DOI: [10.1103/PhysRevB.83.115329](https://doi.org/10.1103/PhysRevB.83.115329)

# Diffusion and interface growth in hafnium oxide and silicate ultra-thin films on Si (001)

L.V. Goncharova,<sup>1\*</sup> M. Dalponte,<sup>1</sup> T. Feng,<sup>1</sup> T. Gustafsson,<sup>1</sup> and E. Garfunkel,<sup>2</sup>

<sup>1</sup>*Departments of Physics and Astronomy, <sup>2</sup>Department of Chemistry and Chemical Biology,  
Rutgers University, 136 Frelinghuysen Rd., Piscataway, New Jersey 08854*

P.S. Lysaght, G. Bersuker

*Sematech, Austin, Texas 78741*

January 24, 2011

## Abstract

Medium energy ion scattering (MEIS) has been used in combination with  $^{16}\text{O}$  and  $^{18}\text{O}$  isotope tracing to determine elemental depth distributions and elucidate oxygen transport in 2-5 nm thick  $\text{HfO}_2$  and  $\text{HfSiO}_x$  films grown by atomic layer deposition on Si(001). Both the oxygen isotope exchange rate in the dielectric as well as the interfacial silicon oxide growth rates were examined as a function of time, temperature, film stoichiometry ( $\text{HfO}_2$ ,  $\text{HfSiO}_x$  and  $\text{HfSiO}_x\text{N}_y$ ) and crystallinity. The amount of exchanged oxygen in the oxide was found to decrease with increasing  $\text{SiO}_2$  content. When the  $\text{SiO}_2$  to  $\text{HfO}_2$  ratio reaches 1:1 in  $\text{HfSiO}_x$  almost full suppression of oxygen exchange is observed. The activation barrier for the  $\text{SiO}_2$  growth at the  $\text{HfO}_2/\text{Si}$  and  $\text{HfSiO}_x/\text{Si}$  interface was found to be much lower than that in the  $\text{SiO}_2/\text{Si}$  and  $\text{SiO}_x\text{N}_y/\text{Si}$  cases, which is attributed to distinctly different oxygen incorporation mechanisms. Primary route for oxygen delivery to the interface responsible for the  $\text{SiO}_2$  growth is via exchange, however direct oxidation by molecular oxygen cannot be discounted completely. In the presence of an interfacial nitride layer the  $^{18}\text{O}$ - $^{16}\text{O}$  exchange is replaced by the  $^{18}\text{O}$ -N exchange, which slows diffusion and reduces the oxidation rate.

**Keywords:** hafnium oxide, silicon oxide, high-resolution depth profiling, silicon

Present address: Department of Physics and Astronomy, University of Western Ontario, London, ON N6A 3K7

## I. Introduction

The continued scaling of microelectronic components has made the introduction of new materials in CMOS technology necessary.<sup>1, 2</sup> Transition metal (Hf, Zr, La) oxides, silicates and ternary Hf-based oxides with a dielectric constant higher than that of SiO<sub>2</sub> are being widely investigated as a dielectric for gate stack and other applications<sup>3, 4</sup> and devices based on such materials are now commercially available from some manufacturers. These new metal oxide based materials often have poor electrical performance (i.e., instability of the threshold potential -  $V_T$ )<sup>5, 6</sup> believed to be connected to the presence of a large number of Si dangling bonds, traps, and other defects at or near the dielectric/Si interface. In order to minimize such interface defects and optimize the electrical characteristics, it has been found to be desirable to have at least one monolayer of SiO<sub>2</sub> at the dielectric/Si interface. The Hf oxide (silicate)/Si interface region is strongly affected by the surface preparation prior to dielectric growth,<sup>7</sup> by growth chemistry, thermal treatment and, often, also by the nature of the metal gate.<sup>8-10</sup> There is a large body of work that addresses issues pertaining to interface preparation and characterization.<sup>7, 8, 11-13</sup>

Although SiO<sub>2</sub> films are thermodynamically stable on Si, some higher- $\kappa$  oxides are not.<sup>1, 3, 14</sup> Additional complications arise from the fact that the overlayer metal-oxygen ratio may not be perfectly stoichiometric during growth. Deposition of high- $\kappa$  oxides on silicon are often accompanied by growth of an interfacial SiO<sub>2</sub> layer, as well as interdiffusion and/or chemical reactions between the overlayers.<sup>15</sup> As a rule, the high- $\kappa$  dielectric stacks require a post-deposition anneal to passivate defects that contribute to current leakage and threshold voltage instability. The anneal ambient may either intentionally be oxygen rich or contain traces of oxygen as in the case of N<sub>2</sub>. Therefore, understanding the process of oxygen incorporation during

post-deposition processing of high- $\kappa$  gate stacks is of critical importance for meeting device performance specifications.

In contrast to  $\text{SiO}_2$ , hafnium oxides and silicates interact strongly with diffusing oxygen, even at relatively low temperatures. Exchange<sup>16</sup> of oxygen from the gas phase with oxygen atoms in the film (which we monitor using oxygen isotopes) occurs throughout the bulk of the high- $\kappa$  film. On the atomic level the fundamental mechanism of O diffusion in ultra-thin ( $\sim 10$ - $30\text{\AA}$ ) hafnium oxide and hafnium silicate layers remains under debate, in particular defining the relative role of oxygen vacancies,<sup>17</sup> interstitial oxygen, molecular vs atomic vs ionic species, grain boundaries, and other modes of transport. Defects in the high- $\kappa$  dielectric layer can not only impact O transport, but they also negatively impact device performance. First-principles calculations show that the most prominent point defects in monoclinic  $\text{HfO}_2$  are positively charged O and negatively charged Hf vacancies.<sup>18</sup> However oxygen interstitials are more important than oxygen vacancies for diffusion processes as the former have a smaller migration barrier.<sup>19</sup> The amorphous  $\text{HfO}_2$  phase has been investigated recently using *ab initio* computational methods to compare the formation and migration of O vacancy, O interstitial, and Hf vacancy point defects in various charge states.<sup>20, 21</sup> The lowest migration barrier was predicted for the positively charged O vacancy. In practice both amorphous and crystalline phase behavior are important since even initially amorphous-grown thin dielectric films is thought to crystallize (Hf oxide)<sup>22</sup> or perhaps even phase separate (Hf silicate)<sup>23</sup> at temperatures comparable with typical processing steps.

If molecular oxygen can diffuse directly to the interface (as it does in  $\text{SiO}_2/\text{Si}$ , perhaps in  $\text{HfO}_2$  via defects or voids) then the oxidation reaction could take place right at the semiconductor interface without reacting with the high- $\kappa$  dielectric.

When oxygen arrives at the lower interface region (regardless of the transport mechanism) it reacts with Si or  $\text{SiO}_{2-x}$  forming  $\text{SiO}_2$ . Additional side reactions are also to be expected, e.g., oxygen arrival to the high- $\kappa$ /Si interface may trigger the injection of Si interstitials from the substrate due to the more open structure in  $\text{SiO}_2$  relative to  $\text{Si}$ .<sup>24</sup> These interstitials can react with oxygen in the  $\text{SiO}_2$  overlayer forming SiO locally which can be removed from the film as observed in  $^{29}\text{Si}$  isotopic tracing experiments,<sup>25</sup> or can be transported into the high- $\kappa$  film, changing its composition.

In this paper we experimentally investigate diffusion and exchange- reactions and growth interface in ultra-thin Hf oxide and silicate films on Si(001). In particular, using high-resolution ion scattering, we have examined a series of different dielectric structures ( $\text{HfO}_2$ ,  $\text{HfSiO}_x$  and  $\text{HfSiO}_x\text{N}_y$ )/Si(001) before and after crystallization annealing, and specifically looked at diffusion of oxygen in these 2-3nm thick films using isotopic tracing. Oxygen exchange and incorporation rates were studied as a function of oxidation time, temperature, film composition (amount of silica in dielectric), crystallinity, and the presence of nitrogen at the interface. We compare our results for the silicon oxide growth rate in  $\text{Hf}_x\text{Si}_{1-x}\text{O}_2/\text{Si}$  with that of growth at the interface of pure 4-5nm  $\text{SiO}_2/\text{Si}$  and  $\text{SiO}_x\text{N}_y/\text{Si}(001)$  studied earlier.<sup>26-28</sup>

## II. Experimental

Hf oxide and silicate films 2-3nm thick were deposited on a 1nm  $\text{SiO}_2/\text{Si}(001)$  or 1 nm  $\text{SiO}_x\text{N}_y/\text{Si}(001)$  film using atomic layer deposition (ALD) at 600K with  $\text{O}_3$  as an oxidation agent.<sup>29</sup> The stoichiometry of  $\text{Hf}_{1-x}\text{Si}_x\text{O}_2$  ( $x = 0, 0.33, 0.67$ ) was controlled by adjusting the relative amounts of hafnia and silica precursors. Nitrogen was introduced into selected samples by postgrowth anneal in  $\text{NH}_3$  (973K, 60s). As a result a 5:1=O:N ratio was achieved. In order to

understand the suppression of the O exchange in Hf silicates, we deposited a  $\sim 2$  ML thick  $\text{SiO}_2$  layer on top of a  $\text{HfO}_2$  film. Postgrowth oxidation in  $^{18}\text{O}_2$  (98% isotopically enriched) was performed *in-situ* in the UHV chamber ( $p_{\text{base}} \sim 10^{-9}$  Torr) connected to the MEIS analysis chamber. The sample was first stabilized at a temperature in the  $\sim 763 - 1223$  K range (measured by an optical pyrometer and or a K-type thermocouple), followed by  $^{18}\text{O}_2$  or  $^{16}\text{O}_2$  gas introduction at a pressure of 0.01 Torr (5 - 30 min).

Medium energy ion scattering was used to determine the depth profile of all elements in the dielectric layers. We used an  $\text{H}^+$  beam with the incident beam normal to the surface. A toroidal electrostatic energy analyzer detector<sup>30</sup> was used centered at a scattering angle of  $125.27^\circ$  corresponding to a high symmetry direction in the substrate. An incident ion energy of 130.8 keV energy was chosen to resolve the  $^{18}\text{O}$  and  $^{16}\text{O}$  peaks,<sup>31</sup> which is close to the maximum stopping power for protons in Si. Depth profiles of all elements were obtained using a computer simulation code of the backscattered ion energy distributions developed by T. Nishimura.<sup>32</sup> The depth resolution is estimated to be  $\sim 3 \text{ \AA}$  at the surface and  $\sim 8 \text{ \AA}$  at a depth of 30  $\text{\AA}$ .<sup>33</sup>

Si,  $^{18}\text{O}$ , and  $^{16}\text{O}$  peaks for all samples were carefully examined to quantitatively determine the depth distribution of both oxygen species and Si throughout the dielectric film. Rates of the silicon oxide growth at the Hf dielectric/ $\text{Si}(001)$  were analyzed, and factors affecting oxygen exchange<sup>26</sup> such as film composition and phase separation were examined.

Complementary x-ray photoemission spectroscopy (XPS) and atomic force microscopy (AFM) measurements were conducted *ex situ*. A commercial XPS system (PHI 5000 series ESCA spectrometer, Al/Mg dual anode source, concentric hemispherical analyzer) was used with a photoelectron take-off angle of  $45^\circ$  and using Al  $K\alpha$  radiation (1486.6 eV). The instrument was calibrated with the Au  $4f_{7/2}$  level at 83.9 eV. Charging, when present, was

corrected by referencing the energy scale to the C1s peak to 285 eV. AFM images were taken under ambient conditions in the “tapping” mode using 125- $\mu\text{m}$  long silicon cantilevers with resonant frequencies  $\sim 250$  kHz.

### III. Results

Figure 1 shows an  $\text{H}^+$  backscattered energy spectrum from an as-deposited  $\text{Hf}_{0.67}\text{Si}_{0.33}\text{O}_2/\text{SiO}_x\text{N}_y/\text{Si}(001)$  film. The proton energies corresponding to the high energy edges of the Hf, Si, O and C (but not N) peaks are in excellent agreement with binary collision model calculations, which means that all these elements can be found at the surface, while the nitrogen is buried. The intensity distribution of Si indicates a concentration variation with depth with a Si peak maximum occurring at an energy corresponding to a depth well below the surface. A simulation of this spectrum showed that the outermost layer of this sample was a stoichiometric  $\text{Hf}_{0.67}\text{Si}_{0.33}\text{O}_2$  film with a thickness of  $27 \pm 2 \text{ \AA}$ . Again, the position of the N peak indicates that there is no N diffusion to the vacuum/ $\text{Hf}_{0.67}\text{Si}_{0.33}\text{O}_2$  interface, and all nitrogen is confined within the interfacial  $\text{SiO}_x\text{N}_y$  layer, while the width of the oxygen peak has contributions from both the Hf silicate and the interfacial layer. A small amount of hydrocarbon contamination at the top surface is apparent from a minor C surface peak.

MEIS data represent averages over a sample area of about  $0.1 \text{ mm}^2$ , making it difficult to distinguish between near interface compositional gradients and interface or surface roughness. Therefore, we performed controlled atomic-force microscopy measurements for selected as-deposited and annealed samples, which revealed rms values of  $\sim 2 \text{ \AA}$  for as-deposited and less than  $5 \text{ \AA}$  for the annealed films.<sup>9</sup>



To investigate the mobility of oxygen, samples were reoxidized in  $^{18}\text{O}_2$  (after having been annealed briefly at 523-573K to remove surface carbon). Postdeposition anneals in  $^{18}\text{O}_2$  were performed at various temperatures, times and film compositions. Our initial findings indicated that at  $\sim 773\text{K}$  interactions between the high- $\kappa$  film and oxygen were limited to exchange reactions, i.e., there is no net increase in oxygen ( $^{16}\text{O} + ^{18}\text{O}$ ) areal densities, therefore no additional  $\text{SiO}_2$  formation.

### A. Exchange reactions

Figure 2a shows the part of the backscattered  $\text{H}^+$  spectrum corresponding to the two oxygen isotopes in  $\text{HfO}_2/\text{SiO}_2/\text{Si}(001)$  films as reoxidation proceeds. A pronounced  $^{18}\text{O}$  peak (spanning from the outer surface of  $\text{HfO}_2$  to the  $\text{SiO}_2$  interfacial layer, as illustrated by the matched  $^{16}\text{O}$  and  $^{18}\text{O}$  peak base energy range) is observed after 10min of  $^{18}\text{O}_2$  exposure ( $p_{^{18}\text{O}_2}=0.01\text{Torr}$ ,  $763\text{K}$ ). Concurrent with the development of the  $^{18}\text{O}$  peak, the intensity of the  $^{16}\text{O}$  peak decreases. This observation shows that the  $^{18}\text{O}$  peak is likely not due to  $^{18}\text{O}_2$  molecular diffusion through the hafnium oxide to the Si interface (as in  $\text{SiO}_2/\text{Si}$ ), but rather due to an exchange reaction in the high- $\kappa$  film, i.e.,  $^{16}\text{O}$  leaves the surface and  $^{18}\text{O}$  goes into the high- $\kappa$  film.<sup>29</sup> After a longer (40 min)  $^{18}\text{O}_2$  exposure there is a larger increase in the  $^{18}\text{O}$  aerial density and decrease in the  $^{16}\text{O}$  density, however, the total oxygen content (sum of  $^{16}\text{O}$  and  $^{18}\text{O}$ ), as calculated from the oxygen peak area, remains the same. (Note that for the same  $^{18}\text{O}$  and  $^{16}\text{O}$  content and distribution, the  $^{18}\text{O}$  peak should have a  $(^{18}/_{16})^2 \sim 1.27$  higher intensity than the  $^{16}\text{O}$  peak, because of the different scattering cross sections.) Based on a full analysis of the Hf, Si and O peak shapes and energies, we conclude that this as-deposited  $\text{HfO}_2$  film has slight excess of oxygen compared to the ideal 1:2 stoichiometry, and a 6-7Å interfacial  $\text{SiO}_2$  layer. Using transmission infra-red spectroscopy, we could also easily detect  $\text{SiO}_2$  (not shown).

$\text{Hf}_{0.67}\text{Si}_{0.33}\text{O}_2/\text{SiO}_x\text{N}_y/\text{Si}(001)$  films behave slightly dissimilar. Under the same processing conditions  $\text{Hf}_{0.67}\text{Si}_{0.33}\text{O}_2/\text{SiO}_x\text{N}_y/\text{Si}(001)$  films (Figure 2b) show a noticeably lower O exchange fraction compared to the  $\text{HfO}_2/\text{SiO}_2/\text{Si}(001)$  films in Fig. 2a. There are no changes in the N, Si and Hf peaks (not shown) for both the Hf oxide and the silicate films, implying that there is no additional interfacial  $\text{SiO}_2$  growth (at these temperatures) and that atomic O diffusion through the interfacial  $\text{SiO}_2$  ( $\text{Si}_3\text{N}_{4-n}\text{O}_n$ ) layer is inefficient under these experimental conditions.

The concentrations of both oxygen isotopes as a function of  $^{18}\text{O}_2$  exposure time are shown Figure 2c. The exchange rate in Hf oxide films (open cycles) was, as mentioned above, faster than for Hf silicates. The oxygen exchange fraction reaches >90% of its final value in 10 min for  $\text{HfO}_2$ , whereas for Hf silicates exchange is much slower and continues, at the listed experimental conditions, even after 120min. We believe the saturation of exchange for the Hf oxide is governed by the onset of the crystallization as discussed below.

In order to quantify and compare the amount of  $^{18}\text{O}$  incorporated into the high- $\kappa$  layer, we estimate the  $^{18}\text{O}$  exchange fraction,  $f$ , as the ratio of  $^{18}\text{O}$  to the total oxygen ( $^{16}\text{O} + ^{18}\text{O}$ ) MEIS areal density in an  $\text{Hf}_{1-x}\text{Si}_x\text{O}_{2-n}\text{N}_n$  films (excluding any interfacial  $\text{SiO}_2$ ). Table I summarizes representative exchange fractions for selected as-deposited and crystalline Hf oxide, silicate and silica oxynitride films. Notably, the oxygen exchange fraction for recrystallized oxides and silicate films are lower than for the as-deposited film. Since the annealing temperature may be sufficient to induce chemical phase separation in this composition of Hf silicate, the lower O exchange fraction observed likely results from a lower surface area of  $\text{HfO}_2$  exposed to oxygen, or a suppression of the diffusion through the silica enriched grain boundaries regions. It is interesting to mention that nitrogen incorporation in the Hf silicates does not change the exchange fraction significantly.

## B. Interfacial silicon oxide growth

For all thin films, as annealing temperatures increase above 763K, interfacial silicon oxide growth is observed in addition to the exchange in the Hf dielectric layer. Fig. 2a and 2b show no net increase in interfacial silicon oxide. The evolution of the Si and O ion scattering peaks for  $\text{Hf}_{0.67}\text{Si}_{0.33}\text{O}_2/\text{SiO}_x\text{N}_y/\text{Si}(001)$  films with the same composition as shown in Fig. 2b at different temperatures (but with the same  $^{18}\text{O}_2$  pressure [0.01 Torr] and anneal time 30 min) is shown schematically in Figure 3. The rise of the Si peak area can be directly associated with the  $\text{SiO}_x$  growth, and will be analyzed separately. The resulting oxygen depth profiles for  $\text{Hf}_{0.67}\text{Si}_{0.33}\text{O}_2/\text{SiO}_x\text{N}_y/\text{Si}(001)$  films are shown in Fig. 4. The thickness of the as-deposited silicate layer is marked by a vertical line. The  $\text{SiO}_2/\text{Si}$  system does not have an atomically sharp interface but changes through a  $\sim 5\text{-}10\text{\AA}$  thick region.<sup>34</sup> We cannot determine the detailed shape of the oxygen distribution due to straggling effects<sup>27, 35</sup>, which become severe for buried layers. Silicon suboxide formation and interfacial layer roughness will both contribute to broadening of the low energy tail of the ion scattering peaks.<sup>27</sup> As the temperature goes up the amount of  $^{18}\text{O}$  exchanged in Hf silicate layer increases, and so does the depth of  $^{18}\text{O}$  incorporation. Oxygen profiles at 973K show a prominent peak at  $\sim 45\text{\AA}$ . This is an artifact of the fitting procedure which assumes that the silicon atomic fraction is constant at 0.33, and therefore the sum of fractions of both oxygen isotopes and nitrogen must be 0.67. Note that since the stoichiometry of the elements in thin films contribute directly to the detected backscattered ion yield, it is a standard assumption in ion beam analysis to keep the sum of the concentrations of all elements in a given layer as 1 (or at least constant). At 973K, the nitrogen content goes to zero at a depth of  $42\text{\AA}$ , therefore both oxygen isotope fractions must go up. In Figure 5 we show the ratio of the  $^{18}\text{O}$  to  $^{16}\text{O}$  content in the Hf-containing layer (the oxygen exchange fraction) as well as in the

interfacial  $\text{SiO}_x$  and  $\text{SiO}_x\text{N}_y$  layer. Two different temperature regimes can be identified. The amount of  $^{18}\text{O}$  in the hafnium silicate (exchange fraction) is increasing continuously as the temperature increases. Yet  $^{16}\text{O}$  is still the predominant oxygen isotope in the interfacial  $\text{SiO}_x$  or  $\text{SiO}_x\text{N}_y$  layer at  $T \leq 973\text{K}$  (no net increase, no oxidation of the Si substrate at this temperature, only isotopic exchange). On the other hand, above  $1000\text{K}$  after 30min annealing the  $^{18}\text{O}$  content at the interface is larger than that of  $^{16}\text{O}$ . Assuming that the only source of  $^{18}\text{O}$  is the gas phase  $^{18}\text{O}_2$ , and  $^{16}\text{O}$  is only in the as-deposited films, we can evaluate how much  $^{16}\text{O}$  is leaving the samples during this incorporation process. From integrating the area of the  $^{16}\text{O}$  peak, we find that we initially have  $^{16}\text{O}$  atomic density of  $10.3 \times 10^{15} \text{ atoms/cm}^2$  in the as-grown Hf silicate films, and that  $6.9 \times 10^{15} \text{ atoms/cm}^2$  remain after  $1223\text{K}$  annealing in  $^{18}\text{O}_2$ . Therefore  $\sim 35\%$  of the  $^{16}\text{O}$  atoms have been removed either via an  $^{16,18}\text{O}_2$  desorption process from  $\text{Hf}_{0.67}\text{Si}_{0.33}\text{O}_2$  surface in direct exchange with gas phase  $^{18}\text{O}_2$ , or via a  $\text{Si}^{16}\text{O}$  desorption from  $\text{SiO}_2/\text{Si}(001)$  interface. Based on our results, an  $^{16,18}\text{O}_2$  desorption process is predominant here, since  $\text{SiO}$  desorption from the  $\text{SiO}_2/\text{Si}$  interface would result in a decrease of the  $\text{SiO}_2$  layer thickness. However  $\text{SiO}$  desorption cannot be excluded completely as a feasible mechanism, and it may become important at higher temperatures.<sup>25, 36</sup> The remaining  $^{16}\text{O}$  is mostly in the interfacial  $\text{SiO}_x\text{N}_y$  layer, as if they have been pushed there by the  $^{18}\text{O}$  atoms from  $\text{Hf}_{0.67}\text{Si}_{0.33}\text{O}_2$  layer.

Selected samples contained nitrogen in the interfacial SiON layer. Therefore we can also compare oxygen isotope distributions and nitrogen depth distributions at various annealing temperatures (Figure 6), for the same samples as shown in Fig. 4 and 5. The total nitrogen content in these films decreases by approximately a factor of two over the temperature range investigated. In addition, the depth distribution broadens quite appreciably. When nitrogen is present, the oxygen distribution extends deeper than the initial nitrogen distribution. The

similarity between the areal densities and profiles of incorporated  $^{18}\text{O}$  (Figure 4b) and lost N (Figure 6) suggests an exchange reaction as a principle mechanism responsible for nitrogen loss and oxygen incorporation.

Figure 7 shows an Arrhenius plot of the interface  $^{18}\text{O}+^{16}\text{O}$  content for three different samples: one with 45Å of starting  $\text{SiO}_2$ , another with 45Å of starting  $\text{SiO}_x\text{N}_y$ , and a third with 27Å  $\text{Hf}_{0.67}\text{Si}_{0.33}\text{O}_2/6\text{ÅSiO}_x\text{N}_y$ , all oxidized in  $^{18}\text{O}_2$  under similar conditions. In these ultrathin films oxidation is presumably “reaction limited”,<sup>37</sup> therefore the interface reaction will be independent of the starting oxide thickness and the increase of  $^{18}\text{O}$  at the interface should depend on both time and pressure linearly. One can see that the rate of oxide growth near the interface is almost one order of magnitude lower for the  $\text{Hf}_{0.67}\text{Si}_{0.33}\text{O}_2/\text{SiO}_x\text{N}_y$  films (compared to pure  $\text{SiO}_2$ ). The Arrhenius plots show straight lines with calculated apparent activation energies of  $2.7\pm0.1\text{eV}$  ( $\text{SiO}_x\text{N}_y/\text{Si}$ ),<sup>26</sup>  $3.0\pm0.1\text{eV}$  ( $\text{SiO}_2/\text{Si}$ ),<sup>26</sup> and  $0.5\pm0.1\text{eV}$  ( $\text{Hf}_{0.67}\text{Si}_{0.33}\text{O}_2/\text{Si}$ ). A lower activation barrier value in the case of hafnium silicate based films is an indication of a distinctly different oxygen incorporation mechanism.

Oxygen interactions with amorphous and crystalline hafnium oxides and silicates were examined in our earlier studies.<sup>29</sup> In addition we note here that crystallization anneals of Hf oxide films at 1023K under UHV conditions results in the development of an additional  $\sim 4\text{-}5\text{Å}$  of  $\text{SiO}_2$  at the lower (dielectric/Si) interface. In XPS, comparison of the Si 2p peaks for pure  $\text{HfO}_2$  films shows that after the 1023K crystallization anneal, the amount of interfacial  $\text{SiO}_2$  increases slightly, consistent with our MEIS observations (Figures 8 and 9). The origin of this additional interfacial  $\text{SiO}_2$  formation will be discussed further below.

## IV. Discussion

## A. Exchange reactions

Our experiments indicated that atomic oxygen diffusion via an oxygen lattice exchange mechanism is the predominant diffusion mechanism in Hf oxide,<sup>29</sup> consistent with theoretical calculations.<sup>19</sup> The *exchange mechanism* involves the continuous replacement of an oxygen lattice site by the diffusing defect (oxygen or vacancy), hence occupancy and exchange of oxygen in lattice sites is the predominant mode of diffusion. Previous experiments with ZrO<sub>2</sub> films<sup>31</sup> and ultra-fine grained ZrO<sub>2</sub>,<sup>38</sup> and density functional calculations of oxygen incorporation and diffusion energies in monoclinic hafnia (HfO<sub>2</sub>)<sup>19</sup> have all suggested that oxygen incorporates and diffuses in atomic (ionic, non-molecular) form. Furthermore, O<sup>2-</sup> becomes a more thermodynamically stable interstitial by accepting two electrons.<sup>19</sup> Calculations by the same authors show that diffusion via oxygen lattice exchange should be the favored mechanism, however the barriers for interstitial oxygen diffusion in HfO<sub>2</sub> are also small, and charged defects could be mobile under high temperature processing conditions. In contrast, molecular oxygen incorporation is preferred for the less dense SiO<sub>2</sub> structure, with diffusion proceeding through interstitial sites.<sup>39</sup>

Provided that the transported species are individual oxygen atoms (or ions), the availability of atomic oxygen at the surface is one of the factors affecting the extent of the exchange in the oxide. O<sub>2</sub> is expected to be adsorbed molecularly on perfect surfaces of HfO<sub>2</sub> and to dissociate primarily at O-vacancy defect (or Hf under-coordinated) sites. The amount of available atomic O depends on the rate of O<sub>2</sub> dissociation at the surface, and is therefore related to the number of oxygen vacancies at the top surface. This brings an interesting possibility of blocking oxygen dissociation by adsorption of a monolayer of SiO<sub>2</sub>. The covalent bonding of this layer will inhibit oxygen dissociation, and therefore inhibits its further diffusion and the

interfacial SiO<sub>2</sub> growth. Additionally, as structural heterogeneity of atoms along the diffusion path may facilitate the lattice exchange of oxygen, as-deposited disordered HfO<sub>2</sub> films might be expected to display a lower diffusion barrier than crystalline films.

We note that kinetics of oxygen exchange (Figure 2) may be controlled to a large extent by crystallization of the as-deposited film occurring in parallel with the exchange. An onset of amorphous Hf oxide crystallization was reported at a temperature as low as 723-773K, resulting in the formation of a monoclinic phase;<sup>22</sup> whereas Hf silicate is stable with respect to phase segregation at these temperatures. During annealing at  $T \geq 1073\text{K}$  Hf silicate films are reported to phase separate into a crystalline HfO<sub>2</sub>-rich phase imbedded in an amorphous silica-rich matrix.<sup>40</sup> Moreover, phase separation in Hf silicates is complex and remains controversial. Some authors have argued that it can proceed by nucleation and growth, or by spinodal decomposition mechanisms dependent on composition and temperature ranges, resulting in different microstructures.<sup>41, 42</sup> There have been no reports of phase separation in the temperature, composition and thickness ranges explored in Figure 2: (773K)/ (Hf<sub>0.67</sub>Si<sub>0.33</sub>O<sub>2</sub>)/ (27Å). While the exchange process is fast for Hf oxide in the first few minutes, it slows down (or stops at a significantly long annealing time (~ 120min)). Considering that (a) <sup>18</sup>O<sub>2</sub> is in excess in the gas phase (10<sup>-2</sup> Torr), (b) the amount of <sup>16</sup>O is limited and well known in as-deposited Hf oxide films, and (c) ~50% of <sup>16</sup>O atoms were exchanged by <sup>18</sup>O in the first 30 min (see table I), one can then expect that >75-80% of oxygen atoms within the Hf oxide framework should be <sup>18</sup>O atoms under the conditions listed above. However this is not the case: <sup>18</sup>O atoms constitute only ~55% of the total oxygen content after 120min of annealing at 763K (Figure 2, c). We speculate that during longer oxidation anneals, when crystallization is completed, and most of the available oxygen dissociation centers at the oxide surface are blocked by bonded oxygen atoms, diffusion

and exchange would proceed predominantly via molecular oxygen incorporation and diffusion via grain boundaries, therefore slowing down the extent of exchange significantly.

Incorporation of nitrogen is a well-known way to reduce diffusion of certain elements, e.g., boron, arsenic and phosphorous diffusion is decreased when nitrogen is incorporated in SiON dielectric layers.<sup>43, 44</sup> In our work nitrogen incorporation into the network of the Hf silicates does not change the exchange fraction of oxygen significantly, if only oxygen atoms are considered in the diffusion process. Therefore the main action of nitrogen is in the reduction of reactive sites for the active species, such as O; the remaining Hf-O-Hf framework will be as active in the oxygen exchange process as it would be in the absence of incorporated nitrogen. Ultimately nitrogen incorporation into the Hf-Si-O network to form HfSiON promotes phase stability and improves electrical performance.<sup>45</sup> Morais et al., showed in XANES that while Hf silicate forms a  $(\text{HfO}_2)_{1-x}(\text{SiO}_2)_x$  pseudobinary alloy upon annealing, while the  $\text{Hf}_{1-x}\text{Si}_x\text{O}_{2-n}\text{N}_n$  system remains amorphous after 1275K, 60s anneal.<sup>45</sup> Since the one of the possible diffusion routes for dopant elements is via grain boundaries, nitrogen incorporation suppresses grain boundary formation during phase segregation and thus dopant diffusion is reduced significantly.<sup>46</sup>

## **B. Growth of the interfacial silicon oxide layer**

The thermodynamics of  $\text{SiO}_x$  layer growth at the interface is controlled by migration of oxygen towards the Si substrate. The rate limiting step in  $\text{HfO}_2/\text{Si}$  interface oxidation appears to be  $\text{O}_2$  going from the gas phase into the  $\text{HfO}_2$  lattice, while in the  $\text{SiO}_2/\text{Si}$  case, the rate limiting step appears to be interstitial  $\text{O}_2$  dissociation and insertion at the  $\text{SiO}_2/\text{Si}$  interface. Once oxygen incorporates at the  $\text{HfO}_2/\text{Si}$  interface, forming a  $\text{HfO}_2/\text{SiO}_2/\text{Si}$  structure, the oxidation rate decreases significantly. The key energy for the oxidation process is the total energy for moving



an oxygen molecule from the gas phase into an interstitial site in the Hf oxide (silicate) in comparison to the insertion energy for the  $\text{SiO}_2/\text{Si}$  case. Our results indicate that the insertion energy is much lower for the former case.

When interstitial oxygen gets to the  $\text{HfSiO}_x/\text{SiO}_2$  interface, at low temperatures ( $<1000\text{K}$ ) it is likely to incorporate in the Si-O-Si- framework forming the  $-\text{Si-O-O-Si}-$  peroxy linkages as in  $\text{SiO}_2$  case.<sup>27, 47, 48</sup> At higher temperatures ( $> 1000\text{K}$ ) additional channels open up for the molecular oxygen to migrate through the grain boundary (or through the more open Si-O-Si network in case of the Hf silicate) to bring molecular  $^{18}\text{O}_2$  to the interface for direct oxidation.<sup>49</sup> This is why (see Figure 7) we suggest there is an increase of  $^{18}\text{O}$  in the interfacial  $\text{SiO}_x$  layer compared to the exchange (in  $\text{HfSiO}_x$ ) fraction above  $1000\text{K}$ .

With regard to interfacial oxide growth, the presence of an interfacial silicon nitride layer modifies the  $^{18}\text{O}$ - $^{16}\text{O}$  into  $^{18}\text{O}$ -N exchange, which slows diffusion and reduces the oxidation rate. When nitrogen is present in the interfacial  $\text{SiO}_x\text{N}_y$  layer, additional  $\text{SiO}_2$  layer growth occurs primarily below the SiON layer. Hence there is a relatively slow  $^{18}\text{O}$ -N displacement exchange in the  $\text{SiO}_x\text{N}_y$  layer. Gavartin, et. al<sup>50</sup> find that nitrogen anneals of high- $\kappa$  dielectric oxides leads to an relative immobilization of defects such as oxygen vacancies and interstitial oxygen ions. In addition to the positive defect passivation benefits of incorporating N in the Si/high- $\kappa$  ( $\text{SiO}_x$ ) interface layer, high N concentrations near the Si substrate interface has been shown to compromise other aspects of device performance and reliability. Our findings illustrate that, although the N depth distribution profile broadens during high temperature annealing in  $^{18}\text{O}$ , N is displaced from the Si substrate during the interfacial  $\text{SiO}_x\text{N}_y$  growth process. This demonstration suggests that accurate control of the Si substrate oxidation may be an effective means of tuning the N concentration profile with respect to the substrate for performance enhancement. Finally

we note that interface growth can result from internal oxygen sources (oxygen trapped in the film during film deposition) as well as external ones. The effect of post-deposition annealing on HfO<sub>2</sub> film composition and HfO<sub>2</sub>/Si interfacial structure clearly shows that SiO<sub>2</sub> starts to develop at the interface as the annealing temperature is raised to 773K *without oxygen in the gas phase*. Therefore we conclude that there are at least two possible oxygen sources for interfacial SiO<sub>2</sub> growth. In addition to relatively slow interfacial growth caused by excess oxygen in the gas phase (external source), for high-κ films growth by atomic layer deposition intrinsic fast sources for interfacial oxide growth may exist: over-stoichiometric oxygen trapped as, for instance, -OH in the dielectric layer (internal source).<sup>7, 51</sup>

## Conclusions

High-resolution ion scattering with isotopic tracing was used to examine oxygen exchange and the mechanism of interfacial growth in hafnium-based ultra-thin dielectric films. The complex oxidation behavior is likely to be a combination of interfacial, near-interfacial, and surface reactions. HfO<sub>2</sub>/SiO<sub>2</sub>/Si(001) samples exposed to <sup>18</sup>O at low temperatures exhibit mostly oxygen exchange (<sup>16</sup>O for <sup>18</sup>O) in the overlayer with no net interfacial oxide growth. The same exposure of the hafnium silicates films also exhibits only isotopic oxygen exchange (no net oxide growth) albeit at a significantly reduced rate, owing to the presence of amorphous HfSiON compared with the grain-boundary-assisted diffusion rate associated with crystalline HfO<sub>2</sub> sample. Exposure of the Hf silicate film system to <sup>18</sup>O at higher temperatures results in a much higher <sup>18</sup>O/<sup>16</sup>O exchange rate throughout the Hf silicate film. Concurrent with the exchange, interfacial SiO<sub>x</sub>N<sub>y</sub> is grown due to the supply of the displaced <sup>16</sup>O (as well as <sup>18</sup>O) that migrates toward the Si substrate; both oxygen isotopes are present at the interface in near equal

abundance. Our findings suggests that an oxidation anneal process may be developed to accurately control the N profile proximity to the Si substrate for performance enhancement.

## Acknowledgements

The work at Rutgers was supported by NSF grant DMR-0706326. We also thank the SRC/Sematech FEP-TC, and CAPES (Brazil) for financial support.

## References

- <sup>1</sup> D. G. Schlom, S. Guha, and S. Datta, MRS Bulletin **33**, 1017 (2008).
- <sup>2</sup> M. M. Frank, S. Kim, S. L. Brown, J. Bruley, M. Copel, M. Hopstaken, M. Chudzik, and V. Narayanan, Microelectr. Eng. **86**, 1603 (2009).
- <sup>3</sup> A. A. Demkov and A. Navrotsky, *Materials Fundamentals of Gate Dielectrics* (Springer, Dordrecht, 2005).
- <sup>4</sup> J. J. Peterson, et al., Electrochem. Solid State Lett. **7**, G164 (2004).
- <sup>5</sup> J. K. Schaeffer, L. R. C. Fonseca, S. B. Samavedam, Y. Liang, P. J. Tobin, and B. E. White, Appl. Phys. Lett. **85**, 1826 (2004).
- <sup>6</sup> M. Copel, Appl. Phys. Lett. **92**, 152909 (2008).
- <sup>7</sup> Y. Wang, M.-T. Ho, L. V. Goncharova, L. S. Wielunski, S. Rivillon-Amy, Y. J. Chabal, T. Gustafsson, N. Moumen, and M. Boleslawski, Chemistry of Materials **19**, 3127 (2007).
- <sup>8</sup> N. Goel, et al., Appl. Phys. Lett. **91**, 113515 (2007).
- <sup>9</sup> L. V. Goncharova, M. Dalponte, T. Gustafsson, O. Celik, E. Garfunkel, P. S. Lysaght, and G. Bersuker, J. Vacuum Sci. Technol. A **25**, 261 (2007).

- 10 H. Kim, P. C. McIntyre, C. O. Chui, C. Saraswat, and S. Stemmer, J. Appl. Phys. **96**, 3467 (2004).
- 11 R. J. Carter, E. Cartier, A. Kerber, L. Pantisano, T. Schram, S. De Gendt, and M. Heyns, Appl. Phys. Lett. **83**, 533 (2003).
- 12 J. C. Hackley, T. Gougousi, and J. D. Demaree, J. Appl. Phys. **102**, 034101 (2007).
- 13 M. P. Agustin, G. B. Bersuker, B. Foran, L. A. Boatner, and S. Stemmer, J. Appl. Phys. **100**, 024103 (2006).
- 14 S. Stemmer, J. Vac. Sci. Technol. B **22**, 791 (2004).
- 15 R. M. C. de Almeida and I. J. R. Baumvol, Surf. Sci. Reports **49**, 1 (2003).
- 16 We define oxygen exchange as substitution of the oxygen atoms within the framework of the thin film by oxygen coming from the gas phase. The number of atoms gained from the gas phase equals to the number of oxygen atoms lost, so total oxygen content of the dielectric remains constant during exchange. This exchange process has to be differentiated from interfacial incorporation and growth, where oxygen reacts with the film or the substrate, increasing the total oxygen content.
- 17 H. S. Baik, M. Kim, G.-S. Park, S. A. Song, M. Varela, A. Franceschetti, S. T. Pantelides, and S. J. Pennycook, Appl. Phys. Lett. **85**, 672 (2004).
- 18 J. X. Zheng, G. Ceder, T. Maxisch, W. K. Chim, and W. K. Choi, Phys. Rev. B **75**, 104112 (2007).
- 19 A. S. Foster, A. L. Shluger, and R. M. Nieminen, Phys. Rev. Lett. **89**, 225901 (2002).
- 20 D. Ceresoli and D. Vanderbilt, Phys. Rev. B **74**, 125108 (2006).
- 21 C. Tang and R. Ramprasad, Phys. Rev. B **81**, 161201 (2010).
- 22 S. V. Ushakov, et al., Phys. Stat. Sol. B **241**, 2268 (2004).

- 23 J. Liu, W. N. Lennard, L. V. Goncharova, D. Landheer, X. Wu, S. Rushworth, and A. C. Jones, J. Electrochem. Society **156**, G89 (2009).
- 24 K. Taniguchi, Y. Shibata, and C. Hamaguchi, J. Appl. Phys. **65**, 2723 (1989).
- 25 I. C. Vickridge, O. Kaitasov, R. J. Chater, and J. A. Kilner, Nucl.Instrum.Meth. B **161-163**, 441 (2000).
- 26 H. C. Lu, Rutgers University, 1997.
- 27 E. P. Gusev, H. C. Lu, T. Gustafsson, and E. Garfunkel, Phys. Rev.B **52**, 1759 (1995).
- 28 H. C. Lu, E. P. Gusev, E. Garfunkel, B. W. Busch, T. Gustafsson, T. W. Sorsch, and M. L. Green, J.Appl.Phys. **87**, 1550 (2000).
- 29 L. V. Goncharova, M. Dalponte, T. Gustafsson, E. Garfunkel, P. S. Lysaght, B. Foran, J. Barnett, and G. I. Bersuker, Appl. Phys. Lett. **89**, 044108 (2006).
- 30 R. M. Tromp, M. Copel, M. C. Reuter, M. Horn von Hoegen, J. Speidell, and R. Koudijs, Rev.Sci.Instrum. **62**, 2679 (1991).
- 31 B. W. Busch, W. H. Schulte, E. Garfunkel, T. Gustafsson, W. Qi, R. Nieh, and J. Lee, Phys.Rev.B **62**, R13 290 (2002).
- 32 T. Nishimura, MEIS simulation program, v. 1.02, Kusatsu Shiga, Japan (2005).
- 33 W. H. Schulte, B. W. Busch, E. Garfunkel, T. Gustafsson, G. Schiwietz, and P. L. Grande, Nucl.Instrum.Meth. B **183**, 16 (2001).
- 34 An estimate of the error of the width of this region is  $\sim 5\text{\AA}$ ; taking into account an additional shift of  $2\text{\AA}$  from the asymmetry of energy straggling, we have a  $\sim 13\pm 5\text{\AA}$  thick transition region, where the oxide structure deviate from the amorphous  $\text{SiO}_2$ .
- 35 N. Bohr and K. Dan, Selsk. Mat. Fys. Medd. **18**, 8 (1948).
- 36 I. J. R. Baumvol, C. Krug, and F. Stedile, Phys. Rev. B **60**, 1492 (1999).

- 37 P. Atkins, *Physical Chemistry*, New York, 1998).
- 38 U. Brossmann, R. Wurschum, U. Sodervall, and H. Schaefer, *J. Appl. Phys.* **85**, 7646 (1999).
- 39 S. Mukhopadhyay, P. V. Sushko, A. M. Stoneham, and A. L. Shluger, *Phys. Rev. B* **71**, 235204 (2005).
- 40 D. A. Neumayer and E. Cartier, *J. Appl. Phys.* **90**, 1801 (2001).
- 41 S. Stemmer, Y. L. Li, B. Foran, P. Lysaght, S. K. Streiffer, P. Fuoss, and S. Seifert, *Appl. Phys. Lett.* **83**, 3141 (2003).
- 42 J. Liu, X. Wu, W. N. Lennard, and D. Landheer, *Phys. Rev. B* **80**, 041403 (2009).
- 43 E. P. Gusev, H. C. Lu, E. Garfunkel, T. Gustafsson, M. L. Green, D. Brasen, and W. N. Lennard, *J. Appl. Phys.* **84**, 2980 (1998).
- 44 M. Quevedo-Lopez, M. El-Bouanani, M. J. Kim, B. E. Gnade, R. M. Wallace, M. R. Visokay, A. Li-Fatou, M. J. Bevan, and L. Colombo, *Appl. Phys. Lett.* **81**, 1609 (2002).
- 45 J. Morais, et al., *Appl. Phys. Lett.* **86**, 212906 (2005).
- 46 C. Driemeier, et al., *Appl. Physics A* **80**, 1045 (2005).
- 47 A. M. Stoneham, M. A. Szymanski, and A. L. Shluger, *Phys. Rev. B* **63**, 241304 (2001).
- 48 M. A. Szymanski, A. L. Shluger, and A. M. Stoneham, *Phys. Rev. B* **63**, 224207 (2001).
- 49 A. M. Stoneham, J. L. Gavartin, and A. L. Shluger, *J. Phys.: Condens. Matter* **17**, 2027 (2005).
- 50 J. L. Gavartin, A. L. Shluger, A. S. Foster, and G. Bersuker, *J. Appl. Phys.* **97**, 053704 (2005).
- 51 M.-T. Ho, Y. Wang, R. T. Brewer, L. S. Wielunski, Y. J. Chabal, N. Moumen, and M. Boleslawski, *Appl. Phys. Lett.* **87**, 133103 (2005).

## Figure captions

FIG. 1. Backscattering spectrum for as-deposited  $\text{Hf}_{0.67}\text{Si}_{0.33}\text{O}_2/\text{SiO}_x\text{N}_y/\text{Si}(001)$  film in channeling alignment.

FIG. 2. Variation of  $^{18}\text{O}$  and  $^{16}\text{O}$  peaks for (a) the  $\text{HfO}_2/\text{SiO}_2/\text{Si}(001)$  and (b) the  $\text{Hf}_{0.67}\text{Si}_{0.33}\text{O}_2/\text{SiO}_x\text{N}_y/\text{Si}(001)$  films as a function of re-oxidation time. (c) Oxygen exchange kinetics curves in hafnium oxide (open symbols) and hafnium silicate (dark symbols) films.

FIG. 3. Schematic representation MEIS spectra for Si,  $^{18}\text{O}$  and  $^{16}\text{O}$  energy range of isotopic exchange and incorporation in hafnium silicate film corresponding to (a) as-deposited film, re-oxidized for 30 min at (b) 763 K, (c) 973 K and (d) 1223 K.

FIG. 4. (a)  $^{16}\text{O}$  and (b)  $^{18}\text{O}$  isotopic depth distributions for hafnium silicate samples oxidized for 30 min at 763-1223K. Depth distribution profiles are deduced from simulations for the MEIS spectra (schematics of the spectra are shown in Fig.3). The thickness of the as-deposited silicate layer is marked by a yellow rectangle. Initial  $\text{Si}_x\text{N}_y/\text{Si}(001)$  interface position is also shown in the as-deposited samples, whereas horizontal arrows indicate spread of N during oxidation. Peaks in O profiles for 973K at  $\sim 45\text{\AA}$  is due to the fitting constraints which assume Si atomic fraction is constant at 0.33, the sum of fractions of O isotopes and nitrogen must be 0.67. When N content goes to zero at the depth of  $42\text{\AA}$ , both O isotopes fractions must go up.

FIG. 5. Variation of oxygen density in (a) hafnium silicate layer and (b) interfacial  $\text{SiO}_x\text{N}_y$  layer is a function of re-oxidation temperature during 30min anneal at  $P_{18\text{O}_2}=10^{-2}\text{Torr}$ .

FIG. 6. Calculated nitrogen distributions in  $\text{Hf}_{0.67}\text{Si}_{0.33}\text{O}_2/\text{SiO}_x\text{N}_y/\text{Si}(001)$  films re-oxidized in  $^{18}\text{O}_2$  at different temperatures. Fractions of the nitrogen atoms,  $y$ , are shown, with the sum for all

the elements adding up to 1. Insert shows integrated nitrogen atom density as a function of re-oxidation temperature.

FIG. 7. Semi-logarithmic dependence of the amount of oxygen atoms incorporated near SiON interface of  $\text{Hf}_{0.67}\text{Si}_{0.33}\text{O}_2/\text{SiO}_x\text{N}_y$  ( $10^{-2}$ Torr, 30min),  $\text{SiO}_x\text{N}_y$  and  $\text{SiO}_2$  (7Torr, 60min) films on the inverse temperature after re-oxidation in  $^{18}\text{O}_2$ .  $\text{SiO}_x\text{N}_y$  and  $\text{SiO}_2$  data are reproduced with the permission .

FIG. 8. Si and O peaks in channeling geometry after crystallization anneal of hafnium oxide film in vacuum. Note that O peak integrated area remains the same, while Si peak increases.

FIG. 9. XPS data for the Si  $2p$  region from  $\text{HfO}_2/\text{SiO}_2/\text{Si}(001)$  (normalized to the  $\text{Si}^0$  peak).



Table I. Areal densities of different oxygen isotopes before and after annealing in  $^{18}\text{O}_2$  atmosphere ( $p_{^{18}\text{O}_2}=10^{-2}\text{Torr}$ ) at  $490^\circ\text{C}$  for 30 min.

Composition	Total oxygen ( $\times 10^{15}$ atoms/ $\text{cm}^2$ )	$^{16}\text{O}$ loss ( $^{18}\text{O}$ gain) ( $\times 10^{15}$ atoms/ $\text{cm}^2$ )	Exchange fraction, $f$
$\text{HfO}_2$	15.6	7.8 ( 7.8 )	0.50
$\text{HfO}_2$ (crystalline)	14.7	5.6 ( 5.8 )	0.40
$\text{Hf}_{0.67}\text{Si}_{0.33}\text{O}_2$	13.3	2.6 ( 2.6 )	0.20
$\text{Hf}_{0.33}\text{Si}_{0.67}\text{O}_2$	14	$< 0.5$ ( 0.5 )	$< 0.04$
$\text{SiO}_2/\text{HfO}_2$	19.5	1.0 (1.0 )	0.07
$\text{Hf}_{0.67}\text{Si}_{0.33}\text{O}_{1.67}\text{N}_{0.33}$	11.0	2.1 (2.1)	0.20

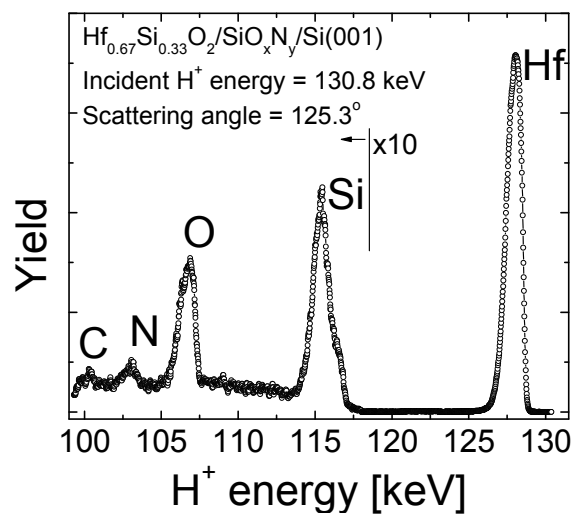


FIG. 1. Backscattering spectrum for as-deposited  $\text{Hf}_{0.67}\text{Si}_{0.33}\text{O}_2/\text{SiO}_x\text{N}_y/\text{Si}(001)$  film in channeling alignment.

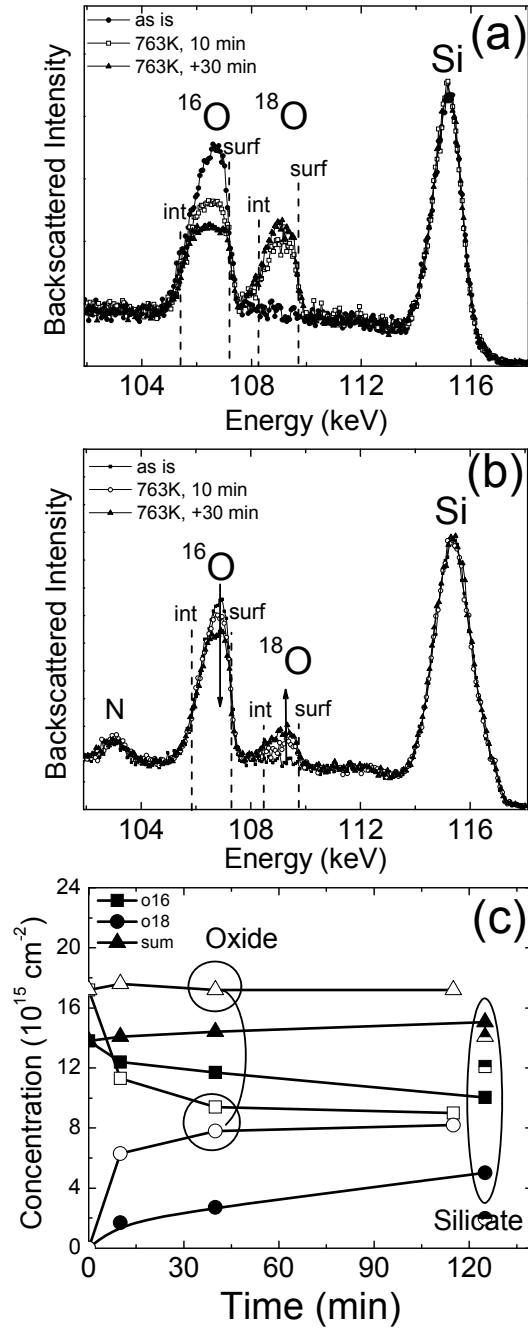


FIG. 2. Variation of  $^{18}\text{O}$  and  $^{16}\text{O}$  peaks for (a) the  $\text{HfO}_2/\text{SiO}_2/\text{Si}$  (001) and (b) the  $\text{Hf}_{0.67}\text{Si}_{0.33}\text{O}_2/\text{SiO}_x\text{N}_y/\text{Si}$ (001) films as a function of re-oxidation time. (c) Oxygen exchange kinetics curves in hafnium oxide (open symbols) and hafnium silicate (dark symbols) films.

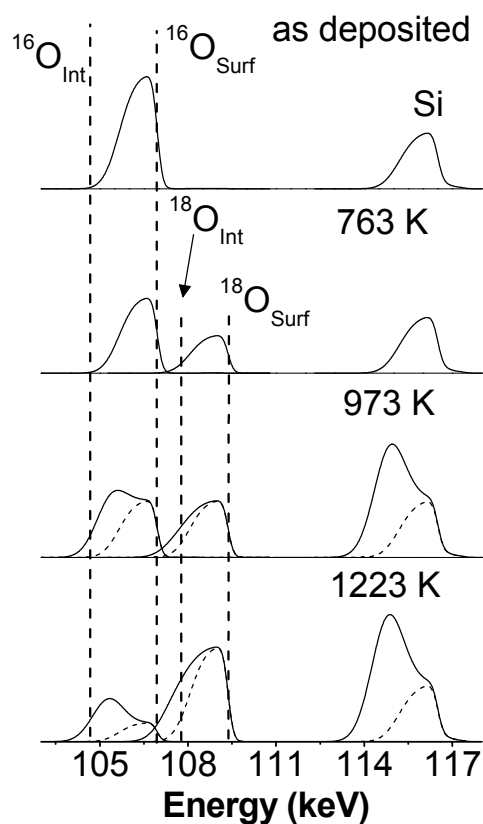


FIG. 3. Schematic representation MEIS spectra for Si,  $^{18}\text{O}$  and  $^{16}\text{O}$  energy range of isotopic exchange and incorporation in hafnium silicate film corresponding to (a) as-deposited film, re-oxidized for 30 min at (b) 763 K, (c) 973 K and (d) 1223 K.

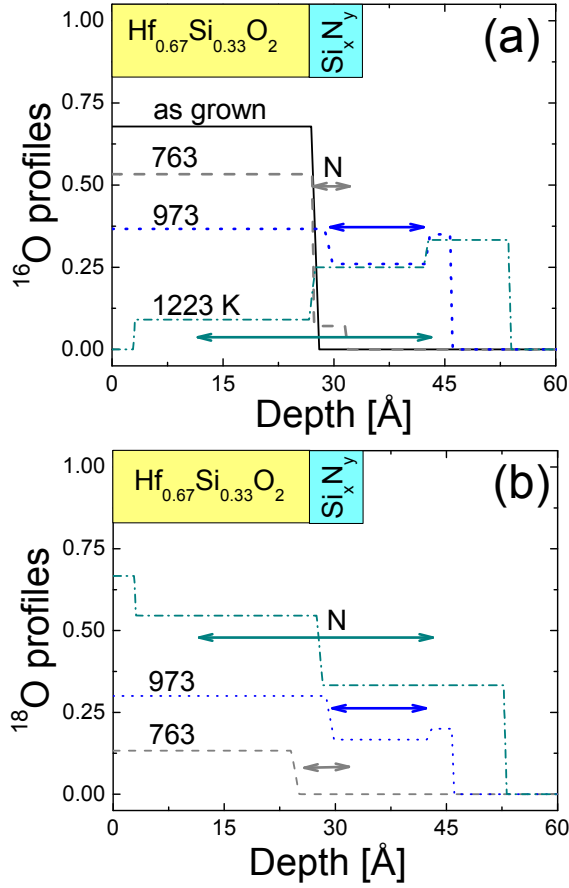


FIG.4. (a)  $^{16}\text{O}$  and (b)  $^{18}\text{O}$  isotopic depth distributions for hafnium silicate samples oxidized for 30 min at 763-1223K. Depth distribution profiles are deduced from simulations for the MEIS spectra (schematics of the spectra are shown in Fig.3). The thickness of the as-deposited silicate layer is marked by a yellow rectangle. Initial  $\text{Si}_x\text{N}_y/\text{Si}(001)$  interface position is also shown in the as-deposited samples, whereas horizontal arrows indicate spread of N during oxidation. Peaks in O profiles for 973K at  $\sim 45\text{\AA}$  is due to the fitting constraints which assume Si atomic fraction is constant at 0.33, the sum of fractions of O isotopes and nitrogen must be 0.67. When N content goes to zero at the depth of  $42\text{\AA}$ , both O isotopes fractions must go up.

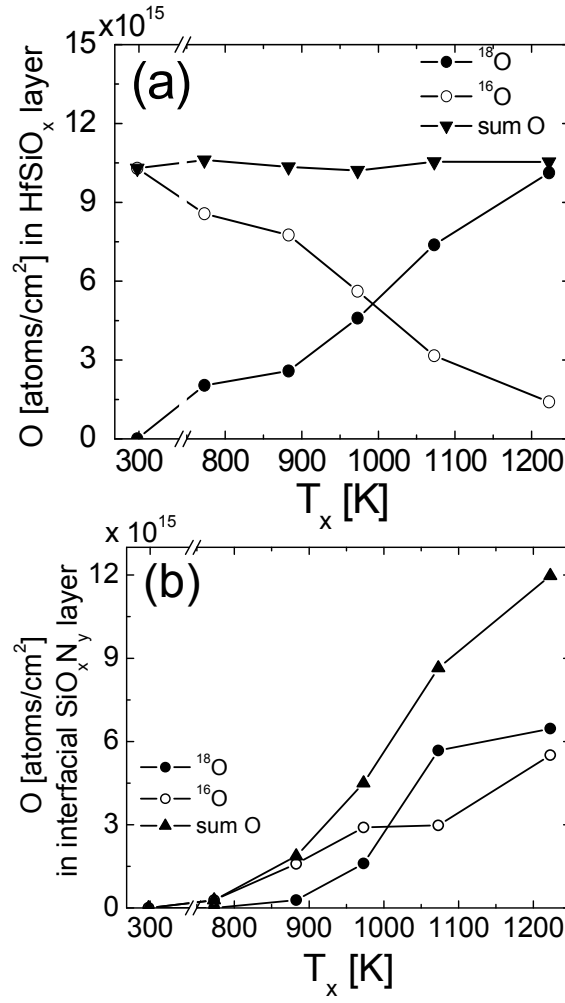


FIG. 5. Variation of oxygen density in (a) hafnium silicate layer and (b) interfacial  $SiO_xN_y$  layer as a function of re-oxidation temperature during 30min anneal at  $P_{18O_2} = 10^{-2}$  Torr.

Figure 6

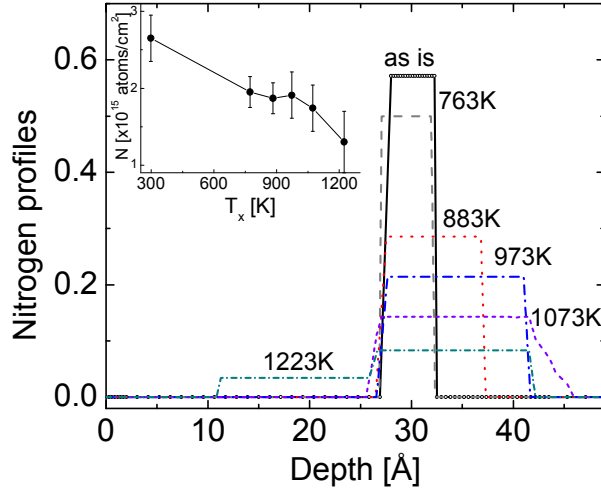


FIG. 6. Calculated nitrogen distributions in  $\text{Hf}_{0.67}\text{Si}_{0.33}\text{O}_2/\text{SiO}_x\text{N}_y/\text{Si}(001)$  films re-oxidized in  $^{18}\text{O}_2$  at different temperatures. Fractions of the nitrogen atoms,  $y$ , are shown, with the sum for all the elements adding up to 1. Insert shows integrated nitrogen atom density as a function of re-oxidation temperature.

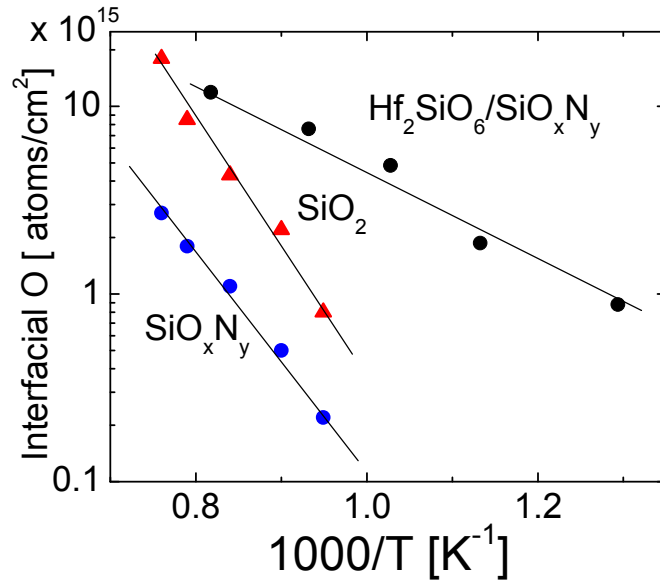


FIG. 7. Semi-logarithmic dependence of the amount of oxygen atoms incorporated near SiON interface of Hf<sub>0.67</sub>Si<sub>0.33</sub>O<sub>2</sub>/SiO<sub>x</sub>N<sub>y</sub> (10<sup>-2</sup>Torr, 30min), SiO<sub>x</sub>N<sub>y</sub> and SiO<sub>2</sub> (7Torr, 60min) films on the inverse temperature after re-oxidation in <sup>18</sup>O<sub>2</sub>. SiO<sub>x</sub>N<sub>y</sub> and SiO<sub>2</sub> data are reproduced with the permission .



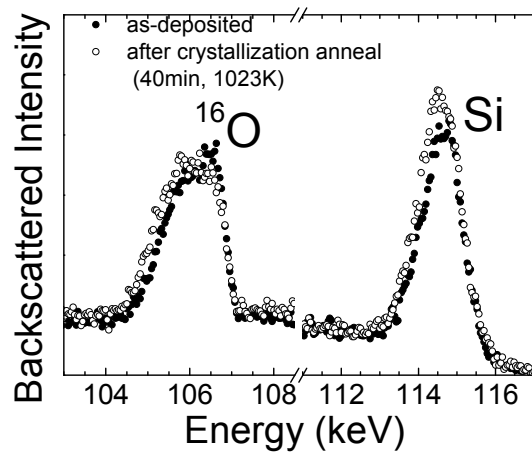


FIG. 8. Si and O peaks in channeling geometry after crystallization anneal of hafnium oxide film in vacuum. Note that O peak integrated area remains the same, while Si peak increases.

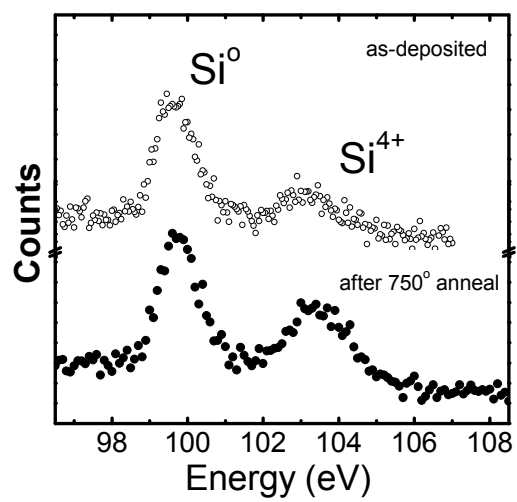


FIG. 9. XPS data for the Si 2*p* region from  $\text{HfO}_2/\text{SiO}_2/\text{Si}(001)$  (normalized to the  $\text{Si}^0$  peak).